Discovery of a Novel HDAC3 Selective Inhibitor and its Evaluation in Lymphoma Model

Chang-Ju Choi,[†,‡] Mira Kim,[†,‡] Sun Young Han,[†] Jiyoung Jeon,[†] Jae Ho Lee,[†] Jeong-In Oh,[†] Kwee Hyun Suh,[†] Dong-Churl Suh,[‡,*] and Kwang-Ok Lee[†,*]

[†]*Department of Drug Discovery, Hanmi Research Center, Hwaseong-si 445-813, Korea. *E-mail: medichem89@gmail.com*
[‡]*College of Pharmacy, Chung-Ang University, Seoul 156-756, Korea. *E-mail: dongsuh75@gmail.com*
Received May 26, 2015, Accepted September 22, 2015, Published online December 17, 2015

Histone deacetylase (HDAC) inhibition is a potentially attractive approach to cancer therapy. A number of HDAC inhibitors are in clinical development stages for the treatment of cancer as well as immune and inflammatory disorders. Although there are several approved HDAC inhibitors by the US FDA, they show a broad inhibitory spectrum against HDAC subfamily. Herein, we synthesized a series of novel hydroxamate analogs, and evaluated them with lymphoma cancer cell. Conclusively, we identified an HDAC3 selective inhibitor which shows good anticancer activity for the lymphoma model, as well as a good drug metabolism and pharmacokinetics (DMPK) profile.

Keywords: HDAC3 selective inhibitor, Lymphoma model

Human histone deacetylases (HDACs) play an important role in regulating the expression and activity of numerous proteins involved in both cancer initiation and cancer progression.[1] More recently, HDACs inhibitors could have utility in the treatment of immune and inflammatory disorders, including rheumatoid arthritis, psoriasis, inflammatory bowel disease (IBD), multiple sclerosis, and systemic lupus erythematosus (SLE).[2] To date, 18 HDAC isoforms have been identified in humans, and they are subdivided into four classes (class I, II, III, and IV).[3]

A number of small molecular HDAC inhibitors are in different stages of clinical development for the treatment of cancer as well as inflammatory disease. Currently, the US FDA has approved three HDAC inhibitors for anticancer drugs (Figure 1). Suberoylanilide hydroxamic acid (SAHA, vorinostat) **1** and romidepsin **2** were approved by the FDA for the treatment of cutaneous T-cell lymphoma (CTCL).[4,5] Recently, another HDAC inhibitor, belinostat **3** has been approved for the treatment of peripheral T-cell lymphoma (PTCL).[6] These approved HDAC inhibitors showed a broad inhibitory spectrum against HDAC subfamily, and their non-selective activity for HDAC subfamily can cause an adverse drug reactions. Despite the proven anticancer effects of HDAC inhibitors against certain cancers, many aspects of HDAC enzymes are still not fully understood. Therefore, the discovery of isoform-selective HDAC inhibitors will ultimately be important for enhancing the safety profile, as well as understanding of the biological activities of each isoform HDAC family.

Recent research indicated, HDAC3 is one of the four members of the human class I HDAC, and it is also overexpressed in various lymphoma cells, as well as play an integral role in regulation of oncoproteins in leukemia and B-cell lymphoma.[7] There are many types of targeted therapies in clinical trials for B-cell lymphoma patients, and two kinase inhibitors that include a BTK inhibitor, ibrutinib, and a PI3K delta inhibitor, idelalisib have recently been approved for the treatment of chronic lymphocyte leukemia (CLL).[8] However, anticancer spectrum of above drugs have limited to partial population of all lymphoma patients.[9] Therefore, a selective HDAC3 inhibitor could be a potential candidate for use with blood cancer therapy, which currently is critically lacking in treatment options. This paper will introduce the synthesis and optimization process of a novel HDAC3 selective inhibitor and its biological evaluation in lymphoma model, as well as its drug metabolism and pharmacokinetics (DMPK) study.

Design and Synthesis

From our in-house screening for the finding of active compound in DOHH-2 lymphoma cell, we confirmed a hit compound **4**, showing GI_{50} as 449 nM (Figure 2). For enhancing the *in vitro* cellular activity, we planned an optimization approach to compound **4** as shown in Figure 2.

First, optimization of part B was done by introducing a linker between phenyl moiety and hydroxamic acid of compound **4** as shown in Scheme 1. Starting material **5** was obtained by the reaction of commercially available cyanuric acid and morpholine, in the presence of triethylamine in acetone (not shown in Scheme 1). Carbon–carbon coupling reaction using a palladium catalyst and 4-aminophenyl boronic acid provided aminophenyl triazine **6**, which was coupled with long chain acids to give intermediate **7**. Finally, terminal methyl ester of intermediate **7** was transformed to

hydroxamate **8** (n = 5), **9** (n = 6), and **10** (n = 7) by the reaction with aqueous hydroxylamine. Also, alkylation of aminophenyl triazine **6** with alkyl bromide afforded methyl ester **11**, which was sequentially converted to hydroxamate **12** as same method of previous hydroxamates. Another carbon–carbon coupling of starting material **5** and 4-hyroxyphenyl boronic acid gave the 4-hydroxy phenyl triazine **13**, which was alkylated to provide methyl ester **14**, and was transformed to hydroxamate **15**.

Lastly, modification of part A was achieved by changing phenyl ring into imidazole or pyrazole that is shown in Scheme 2. For the pyrozole ring, alkylation of pyrazole boronate **16** gave boronate **17** then, a palladium mediated coupling with starting material **5** which provided ester **18**. Finally, the ester group was converted into hydroxamate using the same method as in Scheme 1 to afford the objective compound **19**

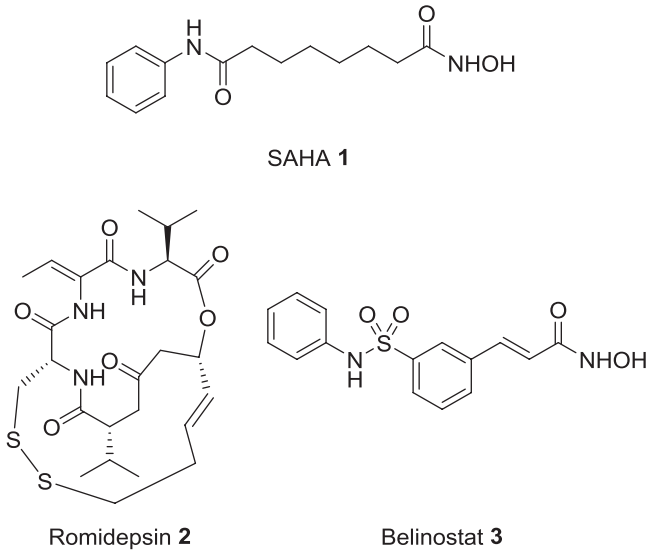

Figure 1. HDAC inhibitors approved by the US FDA.

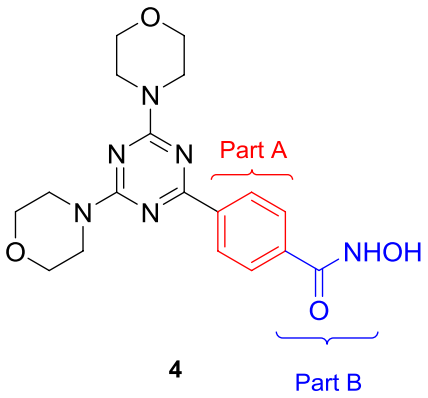

Part A: chanigng into pyrazole or imidazole
Part B: introducing linker between phenyl and hydroxamate

Figure 2. Optimization of compound **4** to enhance the *in vitro* activity in lymphoma cell.

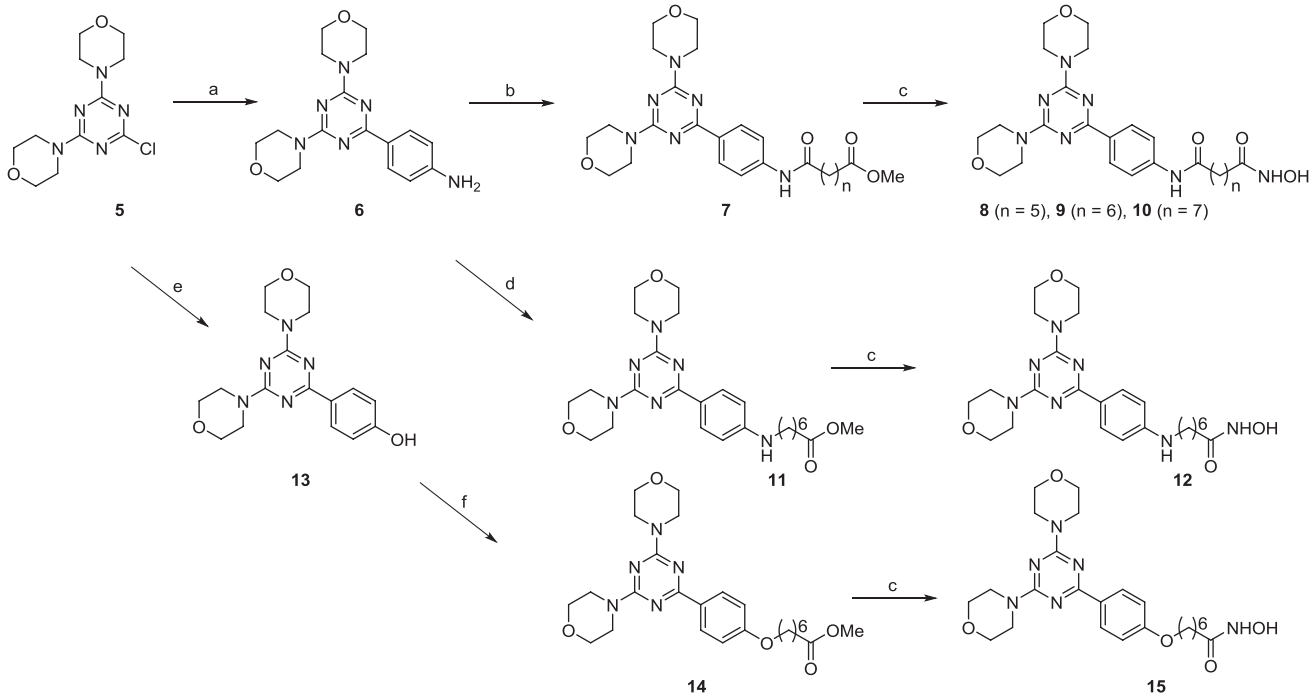

Scheme 1. Reagents and conditions: (a) 4-aminophenyl boronic acid, $Pd(PPh_3)_4$, 2 M Na_2CO_3 (aq.), 1,4-dioxane/H_2O, 90 °C; (b) monomethyl pimelate (n = 5) or monomethyl suberate (n = 6) or monomethyl azelate (n = 7), EDCI, HOBt, DIPEA, DMF, rt; (c) 50% aq. NH_2OH, KCN, THF/MeOH, 60 °C; (d) ethyl 7-bromoheptanoate, NaH, DMF, 0 °C to rt; (e) 4-hydroxyphenyl boronic acid, $Pd(PPh_3)_4$, 2 M Na_2CO_3 (aq.), 1,4-dioxane/H_2O, 90 °C; (f) ethyl 7-bromoheptanoate, K_2CO_3, DMF, 90 °C.

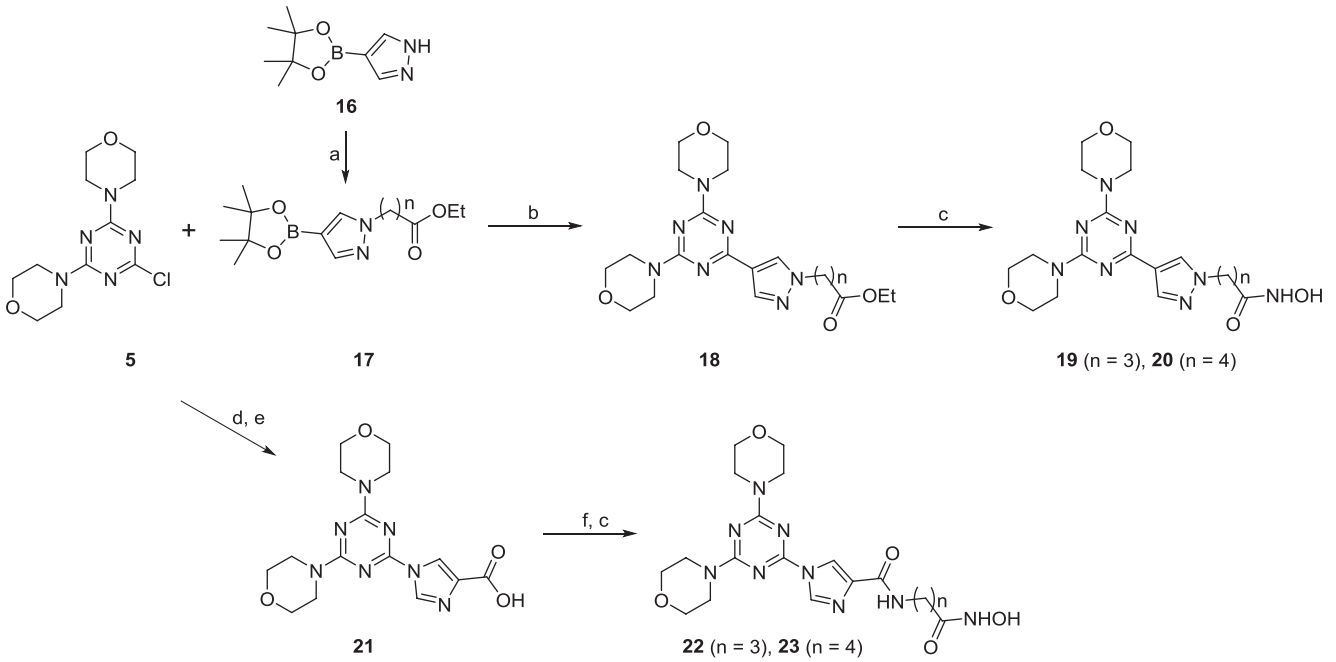

Scheme 2. Reagents and conditions: (a) ethyl 4-bromobutyrate (n = 3) or ethyl 5-bromovalerate (n = 4), NaH, DMF, 0 °C to rt; (b) $Pd(PPh_3)_4$, 2 M Na_2CO_3 (aq.), 1,4-dioxane, 80 °C; (c) 50% aq. NH_2OH, KCN, THF/MeOH, 60 °C; (d) methyl 4-imidazole carboxylate, K_2CO_3, CH_3CN, 60 °C; (e) LiOH, THF/MeOH/H_2O, rt; (f) ethyl 4-aminobutyrate (n = 3) or ethyl 5-aminopentanoate (n = 4), EDCI, HOBt, DIPEA, DMF, rt.

(n = 3) and **20** (n = 4). To introduce an imidazole ring, methyl 4-imidazole carboxylate was coupled with the starting material by general substitution reaction in the presence of K_2CO_3. Then, hydrolysis using lithium hydroxide was done to afford acid **21**. Amidation with ethyl 4-aminobutyrate (n = 3) or ethyl 5-aminopentanoate (n = 4) and following reaction with hydroxyl amine afforded hydroxamate **22** and **23**.

Anticancer and DMPK Evaluation

In this study, nine newly synthesized analogs were screened for the use of the follicular lymphoma cell lines, DOHH-2, and the results summarized in Table 1. Most analogs showed good *in vitro* activities except analog **22** and **23** which have an imidazole group between triazine and hydroxamate. Among analogs **8**, **9**, **10**, **12**, and **15** that have a benzene ring in the region of part A as seen in Figure 2, analog **9**, **12**, and **15** exhibited sub-micromolar cell growth inhibition activity. Although further modification of the linker is needed for the explanation of structure–activity relationships, it seemed that the length of the carbon chain is an important factor to increase *in vitro* cellular activity. Introducing imidazole-4-carboxamide to part A (analogs **22** and **23**) resulted in decreased potency or loss of activity. The result of changed length of aliphatic chain (analog **19**) indicated the decreased potency. It seemed that the length of the carbon chain is an important factor for the activity. The length of aliphatic chain between hydroxamic acid and core is a critical variable in optimizing the positioning of the zinc binding group for HDAC inhibition profiles. Finally, a pyrazole ring was introduced to part A which led to the discovery of analog **20** which shows the most potent *in vitro* activity.[10]

As shown in Table 2, further *in vitro* screening for analog **20** was performed in a variety of lymphoma cancer cells such as follicular lymphoma, activated B-cell type (ABC) diffuse large B-cell lymphoma (DLBCL) and germinal center B-cell type (GCB) DLBCL.[9] Reference compounds including ibrutinib as BTK inhibitor, and idelalisib as PI3K-delta inhibitor, were selected from targeted agents in current clinical stages of lymphoma. These reference compounds demonstrated a narrow spectrum of activity only against TMD-8 (CD79 mutant ABC DLBCL cell line) and DOHH-2 (follicular lymphoma cell line). On the contrary, the analog **20** exhibited a broad spectrum for all lymphoma cancer cells with high *in vitro* potency. For the identification of the role of hydroxamate in the analog **20**, we have synthesized a carboxylic acid substituent to hydroxamate and evaluated *in vitro* activities for DOHH-2 lymphoma cells (data are not shown in this paper). Then we found that the introduction of a carboxylic acid substitution loses the anticancer activity.

Finding the mechanism of action of analog **20**, we screened eleven different HDAC enzymes which shown in Table 3. As most of the HDAC inhibitors have a hydroxamate group as a key interaction of moiety with zinc in the HDAC pocket, we assumed that our analog bind directly to the HDAC enzymes. As expected, analog **20** showed inhibitory activities for eleven HDAC subfamilies. Notably, it showed a potent inhibition

Table 1. *In vitro* activities of triazine analogs in DOHH-2 follicular lymphoma cell.

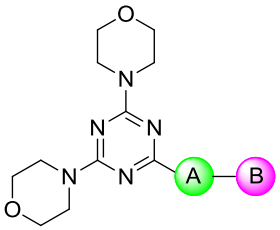

No	A	B	DOHH-2[a] (GI_{50}, μM)
8		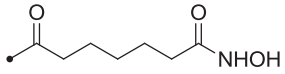	2.15
9		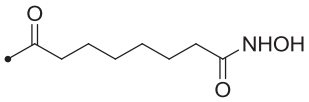	0.18
10	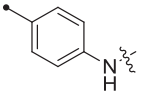	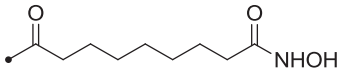	1.76
12		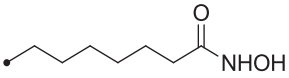	0.85
15		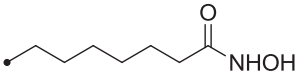	0.30
19	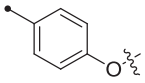	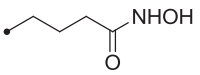	2.44
20	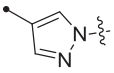	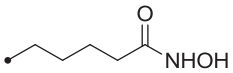	0.020
22		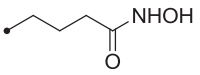	>10
23	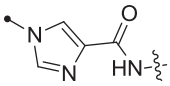	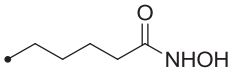	>10

[a] The experiment was performed in duplicate trial.

Table 2. *In vitro* activities of analog **20** in lymphoma cell.

	In vitro cell growth inhibition[a] (GI_{50}, nM)					
	Follicular lymphoma	ABC DLBCL				GCB DLBCL
Compound	DOHH-2	TMD-8[b]	HBL-1[b]	U2932[c]	RC-K8[d]	SU-DHL-4
Ibrutinib[e]	319	1	>10 000	9831	>10 000	1474
Idelalisib[f]	3298	245	>10 000	>10 000	>10 000	1623
Analog **20**	20	3	30	148	94	62

[a] The experiment was performed in duplicate trial.
[b] CD79 mutant cell.
[c] TAK1 mutant cell.
[d] A20 mutant cell.
[e] Ibrutinib: Bruton's tyrosine kinase (BTK) inhibitor.
[f] Idelalisib: PI3K delta kinase inhibitor.

activity for the HDAC3 enzyme with at least a 10-fold increase of selective activity compared with other HDAC enzymes.

We checked drug metabolism and pharmacokinetics (DMPK) of analog **20** before the *in vivo* evaluation which include CYP isozyme (3A4 and 2C9) inhibition, microsomal stability, and plasma stability as shown in Table 4. Analog **20** showed no activities of two CYP isozymes such as 3A4 and 2C9. This result indicated good metabolic stability in human, dog, and rat of liver microsomes and moderate stability in mouse of liver microsome after 1-h incubation. Also, they showed good plasma stability in human, dog, and rat of plasmas, and moderate stability in mouse of plasma after 6-h incubation. As shown in Table 5, a pharmacokinetic study with analog **20** in mice has an oral bioavailability of 19.7%. Also, based on the results of DMPK studies, we concluded that analog **20** is a viable candidate for *in vivo* evaluation as an oral agent.

Finally, *in vivo* evaluation of analog **20** in TMD-8 lymphoma model[11] was done. The *in vivo* efficacy of analog **20** demonstrated a tumor growth inhibition (TGI) rate as 81% (Figure 3). During the period of treatment, any adverse reactions were not observed which include body weight loss.

Table 3. *In vitro* inhibition of HDAC subfamily of analog **20**.

HDAC isoforms	IC_{50} (nM)[a]
1	87
2	133
3	7
4	>10 000
5	>10 000
6	155
7	>10 000
8	2441
9	>10 000
10	272
11	70

[a] HDAC assay was performed at Reaction Biology (Malvern, PA, USA).

Table 4. *In vitro* drug metabolism of analog **20**.

CYP inhibition for 3A4 and 2C9[a] (IC_{50}, μM)	Microsomal stability for four species[b] (mouse/rat/dog/human)	Plasma stability for four species[c] (mouse/rat/dog/human)
>20/>20	66/95/95/94	52/92/88/82

[a] Data were analyzed by rhCYP-fluorescence method.
[b] Remaining percentage of metabolism by incubation of the parent molecule (5 μM) with liver microsomes of mouse, rat, dog, and human for 60 min.
[c] Remaining percentage was measured by incubating the plasma and 0.05 M potassium phosphate buffer (pH 7.4) with parent molecule (0.5 μM, final 0.2% DMSO) for 6 h at 37 °C (400 rpm, n = 3).

Conclusion

In this paper, we synthesized some novel hydroxamate analogs and evaluated their anticancer activity in lymphoma cancer cells. Among the synthesized analogs, analog **20** showed the most potent *in vitro* activities, as well as good *in vivo* efficacy and DMPK profile. Biological assay of analog **20** showed as an HDAC3 selective inhibitor. The establishment of structure–activity relationships is currently undergoing for further modifications. The results will be updated as the research progressed.

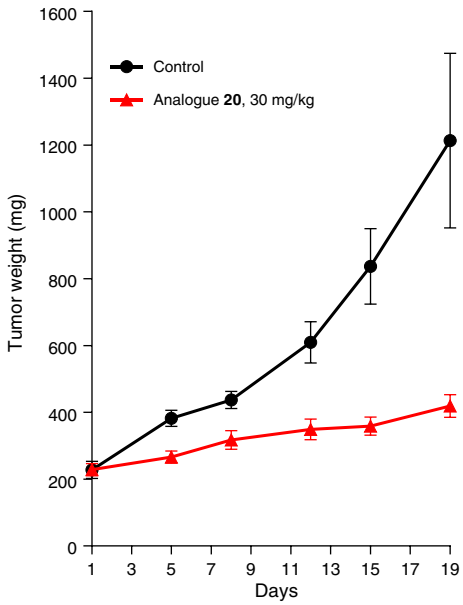

Figure 3. *In vivo* xenograft study of analog **20** in TMD-8 model.

Table 5. Pharmacokinetics of analog **20** in mice.

Pharmacokinetics in mice (n = 3 per time point)[a]						
iv (dose = 5 mg/kg)			*po* (dose = 30 mg/kg)			F (%)
C_0 (ng/mL)	AUC_{INF} (ng · h/mL)	$t_{1/2}$ (h)	C_{max} (ng/mL)	AUC_{INF} (ng · h/mL)	$t_{1/2}$ (h)	
2287.5	363.4	2.0	339.7	431.3	1.1	19.7

[a] Compound was dissolved in a vehicle as a solution of 0.3 M HCl in DMSO, Tween 80, PEG 400, and distilled water (1, 0.5, 1, and 7.5). Pharmacokinetic parameters are calculated from plasma concentration-time data by a noncompartmental method using Phoenix™ WinNonlin® 6.1 (Pharsight, Princeton, NJ, USA).

References

1. (a) M. A. Glozak, E. Seto, *Oncogene* **2007**, *26*, 5420; (b) J. E. Bolden, M. J. Peart, R. W. Johnstone, *Nat. Rev. Drug Discov.* **2006**, *5*, 769; (c) H.-J. Kim, S.-C. Bae, *Am. J. Transl. Res.* **2011**, *3*, 166; (d) A. Mai, S. Massa, D. Rotili, I. Cerbara, S. Valente, R. Pezzi, S. Simeoni, R. Raqno, *Med. Res. Rev.* **2005**, *25*, 261.
2. (a) K. J. Falkenberg, R. W. Johnstone, *Nat. Rev. Drug Discov.* **2014**, *13*, 673; (b) C. Balagué, S. L. Kunkel, N. Godessart, *Drug Discov. Today* **2009**, *14*, 926; (c) S. J. Shuttleworth, S. G. Bailey, P. A. Townsend, *Curr. Drug Targets* **2010**, *11*, 1430.
3. (a) I. V. Gregoretti, Y.-M. Lee, H. V. Goodson, *J. Mol. Biol.* **2004**, *338*, 17; (b) A. J. M. De Ruijter, A. H. Van Gennip, H. N. Caron, S. Kemp, A. B. P. Van Kulenburg, *Biochem. J.* **2003**, *370*, 737.
4. P. A. Marks, R. Breslow, *Nat. Biotechnol.* **2007**, *25*, 84.
5. K. M. VanderMolen, W. McCulloch, C. J. Pearce, N. H. Oberlies, *J. Antibiot.* **2011**, *64*, 525.
6. R. M. Poole, *Drugs* **2014**, *74*, 1543.
7. M. Gupta, J. J. Han, M. Stenson, L. Wellik, T. E. Witzig, *Leukemia* **2012**, *26*, 1356.
8. (a) T. Robak, *Ann. Hematol. Oncol.* **2014**, *1*(1), 1001; (b) A. Markham, *Drugs* **2014**, *74*, 1701.
9. (a) A. L. Shaffer 3rd. , R. M. Young, L. M. Staudt, *Annu. Rev. Immunol.* **2012**, *30*, 565; (b) M. Roschewski, L. M. Staudt, W. H. Wilson, *Nat. Rev. Clin. Oncol.* **2014**, *11*, 12.
10. Spectral data of analog **20**: ^{1}H-NMR (300 MHz, DMSO-d_6) δ 10.35 (s, 1H), 8.68 (s, 1H), 8.34 (s, 1H), 7.97 (s, 1H), 4.13 (t, J = 6.8 Hz, 2H), 3.75 (m, 8H), 3.63 (m, 8H), 1.96 (t, 2H), 1.74 (m, 2H), 1.43 (m, 2H). MS (ESI+): m/z = 433.2 [M+H]+.
11. TMD-8 tumor cells were implanted subcutaneously into female SCID mice. Treatment of tested compounds was initiated when the mean tumor volumes reached 220 mm^3. Analog **20** were administered orally, once a day at doses of 30 mg/kg, respectively. Tumor growth inhibition (TGI) % is defined as: ([$TV_{vehichle}$ Day x – $TV_{vehichle}$ Initial] – [$TV_{treatment}$ Day x – $TV_{treatment}$ Initial]/[$TV_{vehichle}$ Day x – $TV_{vehichle}$ Initial]) × 100%. TV means tumor volume.

